Title	Measurement of branching fractions and CP asymmetries for $D_S^+ \to K^+(\eta, \pi^0)$ and $D_S^+ \to \pi^+(\eta, \pi^0)$ decays at Belle
Author(s)	Guan Y., Tanida Kiyoshi, Belle Collaboration, 202 of others
Citation	Physical Review D, 103(11), p.112005_1-112005_11
Text Version	Published Journal Article
URL	https://jopss.jaea.go.jp/search/servlet/search?5074099
DOI	https://doi.org/10.1103/PhysRevD.103.112005
Right	Published by the American Physical Society under the terms of the Creative Commons Attribution 4.0 International license. Further distribution of this work must maintain attribution to the author(s) and the published article's title, journal citation, and DOI. Funded by SCOAP³.

Measurement of branching fractions and *CP* asymmetries for $D_s^+ \to K^+(\eta,\pi^0)$ and $D_s^+ \to \pi^+(\eta,\pi^0)$ decays at Belle

Y. Guan,[7] A. J. Schwartz,[7] K. Kinoshita,[7] I. Adachi,[19,15] H. Aihara,[88] S. Al Said,[81,38] D. M. Asner,[3] H. Atmacan,[7] V. Aulchenko,[4,65] T. Aushev,[21] R. Ayad,[81] V. Babu,[8] P. Behera,[27] J. Bennett,[52] M. Bessner,[18] V. Bhardwaj,[24] B. Bhuyan,[25] T. Bilka,[5] J. Biswal,[35] G. Bonvicini,[90] A. Bozek,[61] M. Bračko,[49,35] T. E. Browder,[18] M. Campajola,[32,56] D. Červenkov,[5] M.-C. Chang,[10] V. Chekelian,[50] A. Chen,[58] B. G. Cheon,[17] K. Chilikin,[44] K. Cho,[40] S.-K. Choi,[16] Y. Choi,[79] S. Choudhury,[26] D. Cinabro,[90] S. Cunliffe,[8] S. Das,[48] G. De Nardo,[32,56] R. Dhamija,[26] F. Di Capua,[32,56] J. Dingfelder,[2] Z. Doležal,[5] T. V. Dong,[11] S. Eidelman,[4,65,44] D. Epifanov,[4,65] T. Ferber,[8] D. Ferlewicz,[51] A. Frey,[14] B. G. Fulsom,[68] R. Garg,[69] V. Gaur,[89] N. Gabyshev,[4,65] A. Garmash,[4,65] A. Giri,[26] P. Goldenzweig,[36] K. Gudkova,[4,65] C. Hadjivasiliou,[68] S. Halder,[82] T. Hara,[19,15] O. Hartbrich,[18] K. Hayasaka,[63] H. Hayashii,[57] W.-S. Hou,[60] C.-L. Hsu,[80] T. Iijima,[55,54] K. Inami,[54] A. Ishikawa,[19,15] R. Itoh,[19,15] M. Iwasaki,[67] Y. Iwasaki,[19] W. W. Jacobs,[28] S. Jia,[11] Y. Jin,[88] C. W. Joo,[37] K. K. Joo,[6] J. Kahn,[36] A. B. Kaliyar,[82] K. H. Kang,[42] T. Kawasaki,[39] H. Kichimi,[19] C. Kiesling,[50] C. H. Kim,[17] D. Y. Kim,[78] S. H. Kim,[75] Y.-K. Kim,[92] P. Kodyš,[5] T. Konno,[39] A. Korobov,[4,65] S. Korpar,[49,35] E. Kovalenko,[4,65] P. Križan,[45,35] R. Kroeger,[52] P. Krokovny,[4,65] M. Kumar,[48] K. Kumara,[90] A. Kuzmin,[4,65] Y.-J. Kwon,[92] K. Lalwani,[48] J. S. Lange,[12] I. S. Lee,[17] S. C. Lee,[42] P. Lewis,[2] L. K. Li,[7] Y. B. Li,[70] L. Li Gioi,[50] J. Libby,[27] K. Lieret,[46] D. Liventsev,[90,19] C. MacQueen,[51] M. Masuda,[87,72] D. Matvienko,[4,65,44] M. Merola,[32,56] F. Metzner,[36] K. Miyabayashi,[57] R. Mizuk,[44,21] G. B. Mohanty,[82] M. Mrvar,[30] R. Mussa,[33] M. Nakao,[19,15] Z. Natkaniec,[61] A. Natochii,[18] L. Nayak,[26] M. Nayak,[84] N. K. Nisar,[3] S. Nishida,[19,15] K. Nishimura,[18] S. Ogawa,[85] H. Ono,[62,63] Y. Onuki,[88] P. Oskin,[44] P. Pakhlov,[44,53] G. Pakhlova,[21,44] T. Pang,[71] S. Pardi,[32] H. Park,[42] S.-H. Park,[19] S. Patra,[24] S. Paul,[83,50] T. K. Pedlar,[47] R. Pestotnik,[35] L. E. Piilonen,[89] T. Podobnik,[45,35] V. Popov,[21] E. Prencipe,[22] M. T. Prim,[2] M. V. Purohit,[66] M. Röhrken,[8] A. Rostomyan,[8] N. Rout,[27] G. Russo,[56] D. Sahoo,[82] S. Sandilya,[26] A. Sangal,[7] L. Santelj,[45,35] T. Sanuki,[86] V. Savinov,[71] G. Schnell,[1,23] C. Schwanda,[30] Y. Seino,[63] K. Senyo,[91] M. E. Sevior,[51] M. Shapkin,[31] C. Sharma,[48] C. P. Shen,[11] J.-G. Shiu,[60] B. Shwartz,[4,65] F. Simon,[50] J. B. Singh,[69] A. Sokolov,[31] E. Solovieva,[44] S. Stanič,[64] M. Starič,[35] Z. S. Stottler,[89] M. Sumihama,[13] M. Takizawa,[76,20,73] U. Tamponi,[33] K. Tanida,[34] F. Tenchini,[8] K. Trabelsi,[43] T. Uglov,[44,21] Y. Unno,[17] S. Uno,[19,15] P. Urquijo,[51] R. Van Tonder,[2] G. Varner,[18] A. Vossen,[9] E. Waheed,[19] C. H. Wang,[59] M.-Z. Wang,[60] P. Wang,[29] X. L. Wang,[11] S. Watanuki,[43] O. Werbycka,[61] E. Won,[41] X. Xu,[77] B. D. Yabsley,[80] W. Yan,[74] S. B. Yang,[41] H. Ye,[8] J. H. Yin,[41] C. Z. Yuan,[29] Z. P. Zhang,[74] V. Zhilich,[4,65] and V. Zhukova[44]

(Belle Collaboration)

[1]*Department of Physics, University of the Basque Country UPV/EHU, 48080 Bilbao*
[2]*University of Bonn, 53115 Bonn*
[3]*Brookhaven National Laboratory, Upton, New York 11973*
[4]*Budker Institute of Nuclear Physics SB RAS, Novosibirsk 630090*
[5]*Faculty of Mathematics and Physics, Charles University, 121 16 Prague*
[6]*Chonnam National University, Gwangju 61186*
[7]*University of Cincinnati, Cincinnati, Ohio 45221*
[8]*Deutsches Elektronen–Synchrotron, 22607 Hamburg*
[9]*Duke University, Durham, North Carolina 27708*
[10]*Department of Physics, Fu Jen Catholic University, Taipei 24205*
[11]*Key Laboratory of Nuclear Physics and Ion-beam Application (MOE) and Institute of Modern Physics, Fudan University, Shanghai 200443*
[12]*Justus-Liebig-Universität Gießen, 35392 Gießen*
[13]*Gifu University, Gifu 501-1193*
[14]*II. Physikalisches Institut, Georg-August-Universität Göttingen, 37073 Göttingen*
[15]*SOKENDAI (The Graduate University for Advanced Studies), Hayama 240-0193*
[16]*Gyeongsang National University, Jinju 52828*
[17]*Department of Physics and Institute of Natural Sciences, Hanyang University, Seoul 04763*
[18]*University of Hawaii, Honolulu, Hawaii 96822*
[19]*High Energy Accelerator Research Organization (KEK), Tsukuba 305-0801*
[20]*J-PARC Branch, KEK Theory Center, High Energy Accelerator Research Organization (KEK), Tsukuba 305-0801*
[21]*Higher School of Economics (HSE), Moscow 101000*
[22]*Forschungszentrum Jülich, 52425 Jülich*
[23]*IKERBASQUE, Basque Foundation for Science, 48013 Bilbao*

[24]*Indian Institute of Science Education and Research Mohali, SAS Nagar, 140306*
[25]*Indian Institute of Technology Guwahati, Assam 781039*
[26]*Indian Institute of Technology Hyderabad, Telangana 502285*
[27]*Indian Institute of Technology Madras, Chennai 600036*
[28]*Indiana University, Bloomington, Indiana 47408*
[29]*Institute of High Energy Physics, Chinese Academy of Sciences, Beijing 100049*
[30]*Institute of High Energy Physics, Vienna 1050*
[31]*Institute for High Energy Physics, Protvino 142281*
[32]*INFN—Sezione di Napoli, 80126 Napoli*
[33]*INFN—Sezione di Torino, 10125 Torino*
[34]*Advanced Science Research Center, Japan Atomic Energy Agency, Naka 319-1195*
[35]*J. Stefan Institute, 1000 Ljubljana*
[36]*Institut für Experimentelle Teilchenphysik, Karlsruher Institut für Technologie, 76131 Karlsruhe*
[37]*Kavli Institute for the Physics and Mathematics of the Universe (WPI), University of Tokyo, Kashiwa 277-8583*
[38]*Department of Physics, Faculty of Science, King Abdulaziz University, Jeddah 21589*
[39]*Kitasato University, Sagamihara 252-0373*
[40]*Korea Institute of Science and Technology Information, Daejeon 34141*
[41]*Korea University, Seoul 02841*
[42]*Kyungpook National University, Daegu 41566*
[43]*Université Paris-Saclay, CNRS/IN2P3, IJCLab, 91405 Orsay*
[44]*P.N. Lebedev Physical Institute of the Russian Academy of Sciences, Moscow 119991*
[45]*Faculty of Mathematics and Physics, University of Ljubljana, 1000 Ljubljana*
[46]*Ludwig Maximilians University, 80539 Munich*
[47]*Luther College, Decorah, Iowa 52101*
[48]*Malaviya National Institute of Technology Jaipur, Jaipur 302017*
[49]*Faculty of Chemistry and Chemical Engineering, University of Maribor, 2000 Maribor*
[50]*Max-Planck-Institut für Physik, 80805 München*
[51]*School of Physics, University of Melbourne, Victoria 3010*
[52]*University of Mississippi, University, Mississippi 38677*
[53]*Moscow Physical Engineering Institute, Moscow 115409*
[54]*Graduate School of Science, Nagoya University, Nagoya 464-8602*
[55]*Kobayashi-Maskawa Institute, Nagoya University, Nagoya 464-8602*
[56]*Università di Napoli Federico II, 80126 Napoli*
[57]*Nara Women's University, Nara 630-8506*
[58]*National Central University, Chung-li 32054*
[59]*National United University, Miao Li 36003*
[60]*Department of Physics, National Taiwan University, Taipei 10617*
[61]*H. Niewodniczanski Institute of Nuclear Physics, Krakow 31-342*
[62]*Nippon Dental University, Niigata 951-8580*
[63]*Niigata University, Niigata 950-2181*
[64]*University of Nova Gorica, 5000 Nova Gorica*
[65]*Novosibirsk State University, Novosibirsk 630090*
[66]*Okinawa Institute of Science and Technology, Okinawa 904-0495*
[67]*Osaka City University, Osaka 558-8585*
[68]*Pacific Northwest National Laboratory, Richland, Washington 99352*
[69]*Panjab University, Chandigarh 160014*
[70]*Peking University, Beijing 100871*
[71]*University of Pittsburgh, Pittsburgh, Pennsylvania 15260*
[72]*Research Center for Nuclear Physics, Osaka University, Osaka 567-0047*
[73]*Meson Science Laboratory, Cluster for Pioneering Research, RIKEN, Saitama 351-0198*
[74]*Department of Modern Physics and State Key Laboratory of Particle Detection and Electronics, University of Science and Technology of China, Hefei 230026*
[75]*Seoul National University, Seoul 08826*
[76]*Showa Pharmaceutical University, Tokyo 194-8543*
[77]*Soochow University, Suzhou 215006*
[78]*Soongsil University, Seoul 06978*
[79]*Sungkyunkwan University, Suwon 16419*
[80]*School of Physics, University of Sydney, New South Wales 2006*
[81]*Department of Physics, Faculty of Science, University of Tabuk, Tabuk 71451*

[82]*Tata Institute of Fundamental Research, Mumbai 400005*
[83]*Department of Physics, Technische Universität München, 85748 Garching*
[84]*School of Physics and Astronomy, Tel Aviv University, Tel Aviv 69978*
[85]*Toho University, Funabashi 274-8510*
[86]*Department of Physics, Tohoku University, Sendai 980-8578*
[87]*Earthquake Research Institute, University of Tokyo, Tokyo 113-0032*
[88]*Department of Physics, University of Tokyo, Tokyo 113-0033*
[89]*Virginia Polytechnic Institute and State University, Blacksburg, Virginia 24061*
[90]*Wayne State University, Detroit, Michigan 48202*
[91]*Yamagata University, Yamagata 990-8560*
[92]*Yonsei University, Seoul 03722*

(Received 17 March 2021; accepted 27 April 2021; published 9 June 2021)

We report measurements of the branching fractions and *CP* asymmetries for $D_s^+ \to K^+\eta$, $D_s^+ \to K^+\pi^0$, and $D_s^+ \to \pi^+\eta$ decays, and the branching fraction for $D_s^+ \to \pi^+\pi^0$. Our results are based on a data sample corresponding to an integrated luminosity of 921 fb^{-1} collected by the Belle detector at the KEKB e^+e^- asymmetric-energy collider. Our measurements of *CP* asymmetries in these decays are the most precise to date; no evidence for *CP* violation is found.

DOI: 10.1103/PhysRevD.103.112005

Charm hadrons provide a unique opportunity to study charge-parity (*CP*) violation in the up-quark sector. Within the Standard Model (SM), *CP* violation (*CPV*) in charm decays is expected to be small, at the level of 10^{-3} [1,2]. The largest effect is expected to occur in singly Cabibbo-suppressed (SCS) decays [3–5], which receive a contribution from a "penguin" (internal loop) diagram. The only evidence for *CPV* in the charm sector thus far was obtained by the LHCb experiment [6], which measured SCS $D^0 \to K^+K^-$ and $D^0 \to \pi^+\pi^-$ decays. The LHCb result has generated much interest in the literature [1,7,8]. One can also search for *CPV* in Cabibbo-favored (CF) decays; as these decays proceed via tree-level decay amplitudes, an observation of *CPV* would be a clear sign of new physics.

Here we present improved measurements of the branching fractions and *CP* asymmetries for charm decays [9] $D_s^+ \to K^+\eta$, $D_s^+ \to K^+\pi^0$, $D_s^+ \to \pi^+\eta$, and $D_s^+ \to \pi^+\pi^0$. The first two modes are SCS decays, while $D_s^+ \to \pi^+\eta$ is CF, and $D_s^+ \to \pi^+\pi^0$ proceeds via an annihilation amplitude. For this last mode, the branching fraction is expected to be very small [2,10,11], and only an upper limit has been obtained from experiments for its value [12]. The most recent measurements of these branching fractions were made by the CLEO [12] and BESIII [13] experiments. Higher precision measurements would help improve theoretical predictions for *CPV* [1,2,14]. The only measurements of *CPV* in these decays were made by the CLEO experiment [12]; our measurements presented here have significantly improved precision.

We define the *CP* asymmetry in the decay rates as

$$A_{CP} = \frac{\Gamma(D_s^+ \to f) - \Gamma(D_s^- \to \bar{f})}{\Gamma(D_s^+ \to f) + \Gamma(D_s^- \to \bar{f})}, \tag{1}$$

where $\Gamma(D_s^+ \to f)$ and $\Gamma(D_s^- \to \bar{f})$ are the partial decay widths for the final state f and its *CP*-conjugate state $\bar{f}$. As our measured A_{CP} corresponds to charged D mesons, which do not undergo mixing, a nonzero value would indicate *direct CP* violation [15].

Our measurements are based on data recorded by the Belle detector [16] running at the KEKB [17] asymmetric-energy e^+e^- collider. The data samples were collected at e^+e^- center-of-mass (CM) energies corresponding to the $\Upsilon(4S)$ and $\Upsilon(5S)$ resonances, and at 60 MeV below the $\Upsilon(4S)$ resonance. The corresponding integrated luminosities are 711 fb^{-1}, 121 fb^{-1}, and 89 fb^{-1}, respectively. The Belle detector is a large-solid-angle magnetic spectrometer consisting of a silicon vertex detector (SVD), a central drift chamber (CDC), an array of aerogel threshold Cherenkov counters (ACC), a barrellike arrangement of time-of-flight scintillation counters (TOF), and an electromagnetic calorimeter (ECL) consisting of CsI(Tl) crystals. These components are all located inside a superconducting solenoid coil that provides a 1.5 T magnetic field. An iron flux-return located outside of the coil is instrumented to detect K_L^0 mesons and to identify muons.

We calculate signal reconstruction efficiencies, optimize selection criteria, and study various backgrounds using Monte Carlo (MC) simulated events. MC events are generated using EvtGen [18] and PYTHIA [19], and they

are subsequently processed through a detector simulation using GEANT3 [20]. Final-state radiation from charged particles is implemented during event generation using the PHOTOS package [21].

Signal D_s^+ mesons are produced via the process $e^+e^- \to c\bar{c}$, where one of the two charm quarks hadronizes into a D_s^+ (or D_s^-) meson. We also search for a low-momentum photon to reconstruct $D_s^{*+} \to D_s^+\gamma$ decays. Such events, in which a $D_s^{*+} \to D_s^+\gamma$ decay is reconstructed, are referred to as the "tagged" sample. Otherwise, in the case of no reconstructed D_s^{*+} decay, events are referred to as the "untagged" sample [22]. The former has low backgrounds, while the latter has higher statistics. The tagged and untagged samples are statistically independent; i.e., a reconstructed D_s^+ candidate will be in one or the other but not in both. Because the total number of D_s^+ produced in data is not precisely known, we measure the branching fractions of signal modes relative to that of the CF mode $D_s^+ \to \phi(\to K^+K^-)\pi^+$, which has high statistics.

Charged-track candidates are required to originate near the e^+e^- interaction point (IP) and have an impact parameter along the z axis (defined as opposite the e^+ beam direction) of less than 4.0 cm, and in the x-y (transverse) plane of less than 1.0 cm. The tracks are required to have a transverse momentum greater than 100 MeV/c. To identify pion and kaon candidates, a particle identification likelihood is constructed based on energy-loss measurements in the CDC, time-of-flight information from the TOF, and light yield measurements from the ACC [23]. A track is identified as a kaon if the ratio $\mathcal{L}(K)/(\mathcal{L}(K)+\mathcal{L}(\pi)) > 0.6$, where $\mathcal{L}(K)$ and $\mathcal{L}(\pi)$ are the likelihoods that the track is a kaon or pion, respectively. If this criterion is not satisfied, the track is assumed to be a pion. The corresponding efficiencies are approximately 84% for kaons and 94% for pions. Photon candidates are reconstructed from electromagnetic clusters in the ECL that do not have an associated charged track. Such candidates are required to have an energy greater than 50 MeV in the barrel region, and greater than 100 MeV in the end cap region. The hit times of energy deposited in the ECL must be consistent with the beam collision time, as calculated at the trigger level. The photon energy deposited in the 3×3 array of ECL crystals centered on the crystal with the highest energy is required to exceed 80% of the energy deposited in the corresponding 5×5 array of crystals.

Candidate π^0's are reconstructed from photon pairs having an invariant mass satisfying $0.120\ \text{GeV}/c^2 < M_{\gamma\gamma} < 0.150\ \text{GeV}/c^2$; this range corresponds to about 2.5σ in mass resolution. Candidate η mesons are reconstructed via $\eta \to \gamma\gamma$ ($\eta_{\gamma\gamma}$) and $\eta \to \pi^+\pi^-\pi^0$ ($\eta_{3\pi}$) decays. To reduce combinatorial background from low-energy photons, π^0 and $\eta_{\gamma\gamma}$ candidates are required to have $|E_{\gamma_1} - E_{\gamma_2}|/(E_{\gamma_1} + E_{\gamma_2}) < 0.9$, where E_{γ_1} and E_{γ_2} are the energies of the two photons. If a photon can pair with another photon to form a π^0 candidate, then it is not used to reconstruct $\eta_{\gamma\gamma}$ candidates. The invariant masses of $\eta_{\gamma\gamma}$ and $\eta_{3\pi}$ candidates are required to satisfy $0.500\ \text{GeV}/c^2 < M_{\gamma\gamma} < 0.580\ \text{GeV}/c^2$ and $0.538\ \text{GeV}/c^2 < M_{\pi^+\pi^-\pi^0} < 0.557\ \text{GeV}/c^2$, respectively; these ranges correspond to about 3.0σ in mass resolution. Mass-constrained fits are performed for π^0, $\eta_{\gamma\gamma}$, and $\eta_{3\pi}$ candidates to improve their momentum resolution. For the reference mode $D_s^+ \to \phi\pi^+$, ϕ candidates are reconstructed from K^+K^- pairs that form a vertex and have an invariant mass satisfying $1.010\ \text{GeV}/c^2 < M_{K^+K^-} < 1.030\ \text{GeV}/c^2$. We also reconstruct $K_S^0 \to \pi^+\pi^-$ decays, as the multiplicity of such decays (and also K^+ candidates) is used later by a neural network to reduce backgrounds. These candidates are reconstructed from $\pi^+\pi^-$ pairs that form a vertex and satisfy $|M_{\pi^+\pi^-} - m_{K_S^0}| < 20\ \text{MeV}/c^2$, where $m_{K_S^0}$ is the nominal mass of the K_S^0 [24].

We subsequently reconstruct D_s^+ candidates by combining a K^+ or π^+ track with a π^0, $\eta_{\gamma\gamma}$, or $\eta_{3\pi}$ candidate. For $D_s^+ \to \phi\pi^+$ decays, we combine a π^+ track with a ϕ candidate. For $D_s^+ \to (K^+, \pi^+)\pi^0$ and $D_s^+ \to \pi^+\eta_{\gamma\gamma}$ decays, we require that the invariant mass satisfy $1.86\ \text{GeV}/c^2 < M_{D_s^+} < 2.07\ \text{GeV}/c^2$; for $D_s^+ \to K^+(\eta_{\gamma\gamma}, \eta_{3\pi})$ and $D_s^+ \to \pi^+\eta_{3\pi}$, we require $1.86\ \text{GeV}/c^2 < M_{D_s^+} < 2.05\ \text{GeV}/c^2$. A narrower range is chosen for $D_s^+ \to K^+(\eta_{\gamma\gamma}, \eta_{3\pi})$ in order to avoid an excess of events in the region $M > 2.05\ \text{GeV}/c^2$ originating from $D_s^+ \to \pi^+\eta$ decays, with the π^+ misidentified as a K^+. A narrower range is chosen for $D_s^+ \to \pi^+\eta_{3\pi}$ due to its better resolution.

For the reference mode $D_s^+ \to \phi\pi^+$, we require $1.93\ \text{GeV}/c^2 < M_{D_s^+} < 2.01\ \text{GeV}/c^2$. In addition, for $D_s^+ \to (K^+, \pi^+)\eta_{3\pi}$ and $D_s^+ \to \phi\pi^+$ decays, we require that the charged tracks form a vertex. To suppress combinatorial backgrounds and also D_s^+ candidates originating from B decays, we require that the D_s^+ momentum in the e^+e^- CM frame be greater than 2.3 GeV/c.

We reconstruct D_s^{*+} candidates by combining a D_s^+ candidate with a γ. The γ is required to have an energy $E_\gamma > 0.15$ GeV and not be associated with a π^0 candidate. The mass difference $\Delta M \equiv M_{D_s^+\gamma} - M_{D_s^+}$, where $M_{D_s^+}$ is the invariant mass of the D_s^+ candidate, is required to satisfy $0.125\ \text{GeV}/c^2 < \Delta M < 0.155\ \text{GeV}/c^2$. The upper and lower ranges correspond to about 2.5σ and 3.5σ in resolution, respectively. The lower range is larger due to a longer tail in the distribution of γ energy. The D_s^+ candidates that satisfy the above $D_s^{*+} \to D_s^+\gamma$ requirements constitute the tagged sample.

To suppress backgrounds, we use a neural network (NN) [25] based on the following input variables. *(1)* The momentum of the D_s^+ in the CM frame. *(2)* $|dl_{xy}|$ or $|dr|$, where $|dl_{xy}|$ is the distance in the x-y plane (transverse to the e^+ beam) between the D_s^+ decay vertex and its production vertex. The latter is taken to be the e^+e^- IP. For modes in which there is only one charged track, the D_s^+

decay vertex cannot be reconstructed; in this case, we use the variable $|dr|$, which is the impact parameter of the charged track in the x-y plane with respect to the IP. *(3)* The cosine of the helicity angle θ_h, which is the angle in the D_s^+ rest frame between the momentum of the K^+ or π^+ daughter and the opposite of the boost direction of the lab frame. *(4)* The number of $K^\pm$ and K_S^0 candidates reconstructed recoiling against the signal D_s^+ candidate. For $e^+e^- \to c\bar{c}$ events, the charm quark that does not hadronize to the signal D_s^+ typically produces a kaon via a $c \to s$ transition. *(5)* The angle between the D_s^+ momentum and the thrust axis of the event, both evaluated in the CM frame. The thrust axis ($\hat{t}$) is defined as the unit vector that maximizes the quantity $\sum_i |\hat{t} \cdot \vec{p}_i| / \sum_i |\vec{p}_i|$, where $\vec{p}_i$ are the momenta of particles, and i runs over all particles in the event. For $e^+e^- \to c\bar{c}$ events, D_s^+ mesons tend to be produced with high momentum, and thus their direction tends to be close to that of $\hat{t}$. *(6)* The angle between the D_s^+ momentum and the vector joining its decay vertex and its production vertex in the x-y plane. This variable is available only for $D_s^+ \to (K^+, \pi^+)\eta_{3\pi}$ and $D_s^+ \to \phi\pi^+$ decays, i.e., modes with more than one charged track in the final state.

The NN outputs a single variable ($O_{\rm NN}$), which ranges from -1 to $+1$. Events with values close to $+1$ (-1) are more signallike (backgroundlike). For each signal mode, we require that $O_{\rm NN}$ be greater than some minimum value, which is determined by optimizing a figure-of-merit (FOM). The FOM is taken to be the ratio $N_{\rm sig}/\sqrt{N_{\rm sig} + N_{\rm bkg}}$, where $N_{\rm sig}$ and $N_{\rm bkg}$ are the expected yields of signal and background events, respectively. The former is evaluated via MC simulation, using world-average values of branching fractions for signal modes [24]. The latter is evaluated by scaling events in data that are reconstructed in a mass sideband. This sideband is defined as $2.04\ {\rm GeV}/c^2 < M_{D_s^+} < 2.10\ {\rm GeV}/c^2$ for $D_s^+ \to (K^+, \pi^+)\pi^0$ and $D_s^+ \to (K^+, \pi^+)\eta_{\gamma\gamma}$; $2.02\ {\rm GeV}/c^2 < M_{D_s^+} < 2.05\ {\rm GeV}/c^2$ for $D_s^+ \to K^+\eta_{3\pi}$; and $2.02\ {\rm GeV}/c^2 < M_{D_s^+} < 2.10\ {\rm GeV}/c^2$ for $D_s^+ \to \pi^+\eta_{3\pi}$. For $D_s^+ \to \pi^+\pi^0$ decays, the branching fraction is unknown; thus, for this mode the FOM is taken to be $\varepsilon_{\rm sig}/\sqrt{N_{\rm bkg}}$, where $\varepsilon_{\rm sig}$ is the reconstruction efficiency [26]. The final selection criteria range from $O_{\rm NN} > 0.70$ for $D_s^+ \to \pi^+\eta_{3\pi}$ to $O_{\rm NN} > 0.94$ for $D_s^+ \to \pi^+\pi^0$. The corresponding signal efficiencies range from 35% for $D_s^+ \to \pi^+\pi^0$ to 63% for $D_s^+ \to \pi^+\eta_{3\pi}$.

A small fraction of events have multiple D_s^+ candidates. This fraction ranges from 1% to 5%, depending on the decay mode. For such events, we select one candidate in an event by choosing the one with the smallest χ^2 resulting from the mass-constrained fit of the η or π^0 decay. If, after this selection, there are still multiple candidates, we choose the one with the highest value of $O_{\rm NN}$. For the reference mode $D_s^+ \to \phi\pi^+$, which has no η or π^0 in the final state, we choose the candidate with the highest $O_{\rm NN}$. The efficiency of this best-candidate selection is evaluated from MC simulation to be about 70%.

The number of signal events is obtained from an unbinned maximum likelihood fit to the D_s^+ mass distribution. For each mode, we perform a simultaneous fit to the $M_{D_s^+}$ distributions of both the tagged and untagged samples. The nominal fitting range is 1.86–$2.07\ {\rm GeV}/c^2$. However, for $D_s^+ \to K^+(\eta_{\gamma\gamma}, \eta_{3\pi})$ and $D_s^+ \to \pi^+\eta_{3\pi}$, the range is 1.86–$2.05\ {\rm GeV}/c^2$. We fit the D_s^+ and D_s^- samples separately but simultaneously.

The following probability density functions (PDFs) are used for fitting signal and background components. For the signal component, the sum of a Crystal Ball (CB) function [27] and a Gaussian function, with both having the same mean, is used. For $D_s^+ \to \pi^+\eta_{\gamma\gamma}$ and $D_s^+ \to \pi^+\eta_{3\pi}$, which have high statistics, the common mean and the widths are floated. For other signal modes, the means are fixed to those from $D_s^+ \to \pi^+\eta$, while the widths are fixed to MC simulation values that are scaled to account for differences in resolution between data and the MC. The scaling factors are determined by comparing signal shape parameters between data and MC simulation for $D_s^+ \to \pi^+\eta$. The relative fraction of the Gaussian function and two remaining parameters of the CB function are fixed to MC simulation values.

The dominant background is combinatorial, for which a second-order Chebyshev polynomial is used. All background parameters are floated. The decays $D^+ \to (K^+, \pi^+)\pi^0$ and $D^+ \to (K^+, \pi^+)\eta$ form peaks in the $D_s^+ \to (K^+, \pi^+)\pi^0$ and $D_s^+ \to (K^+, \pi^+)\eta$ mass distributions; these peaks are described by Gaussian functions. The $D^+ \to \pi^+\pi^0$ and $D^+ \to \pi^+\eta$ decays also form peaks in the $D_s^+ \to K^+\pi^0$ and $D_s^+ \to K^+\eta$ mass distributions (albeit very small) when the π^+ is misidentified as a K^+. The shape of this background and the fractions of $D^+ \to \pi^+\pi^0$ and $D^+ \to \pi^+\eta$ decays that are misidentified are taken from MC simulation. The yields of $D^+ \to \pi^+\pi^0$ and $D^+ \to \pi^+\eta$ are obtained from the fits to the $\pi^+\pi^0$ and $\pi^+\eta$ mass distributions.

For the reference mode $D_s^+ \to \phi\pi^+$, the signal PDF is the sum of a bifurcated Student's t-distribution [28] and a Gaussian function. The mean and width of the signal peak and the fraction of the Gaussian function are floated. There is a small background from $D_s^+ \to K^+K^-\pi^+$, in which the kaons do not originate from $\phi \to K^+K^-$. As this background has the same mass distribution as $D_s^+ \to \phi\pi^+$, it cannot be distinguished from the latter in the fit. We thus correct the $\phi\pi^+$ yield to account for the $K^+K^-\pi^+$ contribution. This contribution is estimated from MC simulation to be $(1.73 \pm 0.03)\%$ [29].

The $M_{D_s^+}$ distributions along with projections of the fit result are shown in Figs. 1, 2, and 3. The branching fraction $\mathcal{B}_{\rm sig}$ for the signal modes is calculated as

$$\mathcal{B}_{\rm sig} = \left(\frac{N_{\rm sig}}{N_{\phi\pi^+}}\right)\left(\frac{\varepsilon_{\phi\pi^+}}{\varepsilon_{\rm sig}}\right)\cdot\mathcal{B}_{\phi\pi^+}, \tag{2}$$

where $N_{\rm sig}$ and $N_{\phi\pi^+}$ are the yields of the signal and reference mode $D_s^+ \to \phi\pi^+$, respectively. Each yield is the sum of the yields for the tagged and untagged samples. The terms $\varepsilon_{\rm sig}$ and $\varepsilon_{\phi\pi^+}$ are the corresponding reconstruction efficiencies, as evaluated from MC simulation. The branching fraction $\mathcal{B}_{\phi\pi^+}$ for $D_s^+ \to \phi(\to K^+K^-)\pi^+$ is taken to be the world-average value $(2.24 \pm 0.08)\%$ [24].

All signal yields and resulting branching fractions are listed in Table I. A weighted average of the results from the two η decay channels ($\eta_{\gamma\gamma}$ and $\eta_{3\pi}$) is also given. The results listed include systematic uncertainties, which are discussed later. As no significant signal for $D_s^+ \to \pi^+\pi^0$ is observed, we set an upper limit on its branching fraction using a Bayesian approach. We calculate the likelihood function $\mathcal{L}$ as a function of branching fraction; the value ξ that satisfies $\int_0^\xi \mathcal{L}(x)dx = 0.90$ is taken to be the 90% confidence level (C.L.) upper limit. We include systematic uncertainty into this limit by convolving $\mathcal{L}(x)$, before integrating, with a Gaussian function whose width is equal to the total systematic uncertainty. The result is $\mathcal{B}(D_s^+ \to \pi^+\pi^0) < 1.2 \times 10^{-4}$ at 90% C.L.

As the D_s^+ and D_s^- samples are fitted separately, we obtain the raw asymmetry $A_{\rm raw}$, defined as

$$A_{\rm raw} = \frac{N_{D_s^+} - N_{D_s^-}}{N_{D_s^+} + N_{D_s^-}}. \tag{3}$$

In this expression, $N_{D_s^+}$ ($N_{D_s^-}$) is the signal yield for the D_s^+ (D_s^-) sample. This raw asymmetry receives three contributions,

$$A_{\rm raw} = A_{CP} + A_{\rm FB} + A_\epsilon, \tag{4}$$

where A_{CP} is the intrinsic CP asymmetry of interest; $A_{\rm FB}$ is the "forward-backward" asymmetry that arises from interference between amplitudes mediated by a virtual photon and by a Z^0 boson; and A_ϵ is an asymmetry that arises from a difference in reconstruction efficiencies between positively charged and negatively charged tracks. The asymmetry $A_{\rm FB}$ is an odd function of the cosine of the D_s^+ polar angle in the CM frame ($\cos\theta_{D_s}^{\rm CM}$). The asymmetry A_ϵ arises from small differences in tracking and particle identification efficiencies and depends on the momentum and polar angle of the charged track. For $D_s^{*+} \to D_s^+\gamma$ decays, we find that the momentum distribution of the π^+ or K^+ in the D_s^+ decay is essentially the same as that in prompt D_s^+ decays. Thus, for a D_s^+ decay mode, we take A_ϵ to be the same for both the tagged and untagged samples.

For the mode $D_s^+ \to \pi^+\eta$, we correct for $A_{\rm FB}$ and A_ϵ using the reference mode $D_s^+ \to \phi\pi^+$. As the momentum spectrum and polar angle distributions of the π^+ daughters

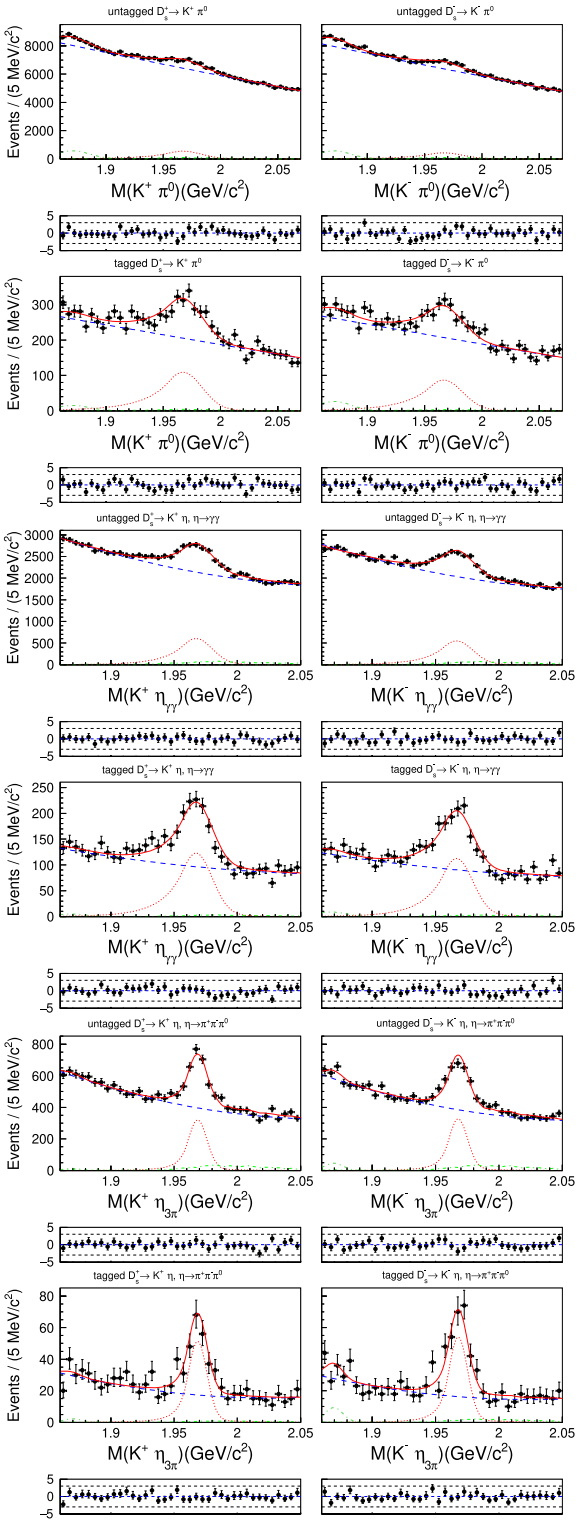

FIG. 1. Data and fit projection for $D_s^+ \to K^+\pi^0$ (upper two rows), $D_s^+ \to K^+\eta_{\gamma\gamma}$ (middle two rows), and $D_s^+ \to K^+\eta_{3\pi}$ (lower two rows). Left side shows D_s^+ candidates, right side shows D_s^- candidates. For each pair of rows, top is the untagged sample, bottom is the tagged sample. The solid red line is the total fit, the dotted red line is signal, the broken green line is background from D^+, and the dashed blue line is combinatorial background. The plots beneath the distributions show the residuals.

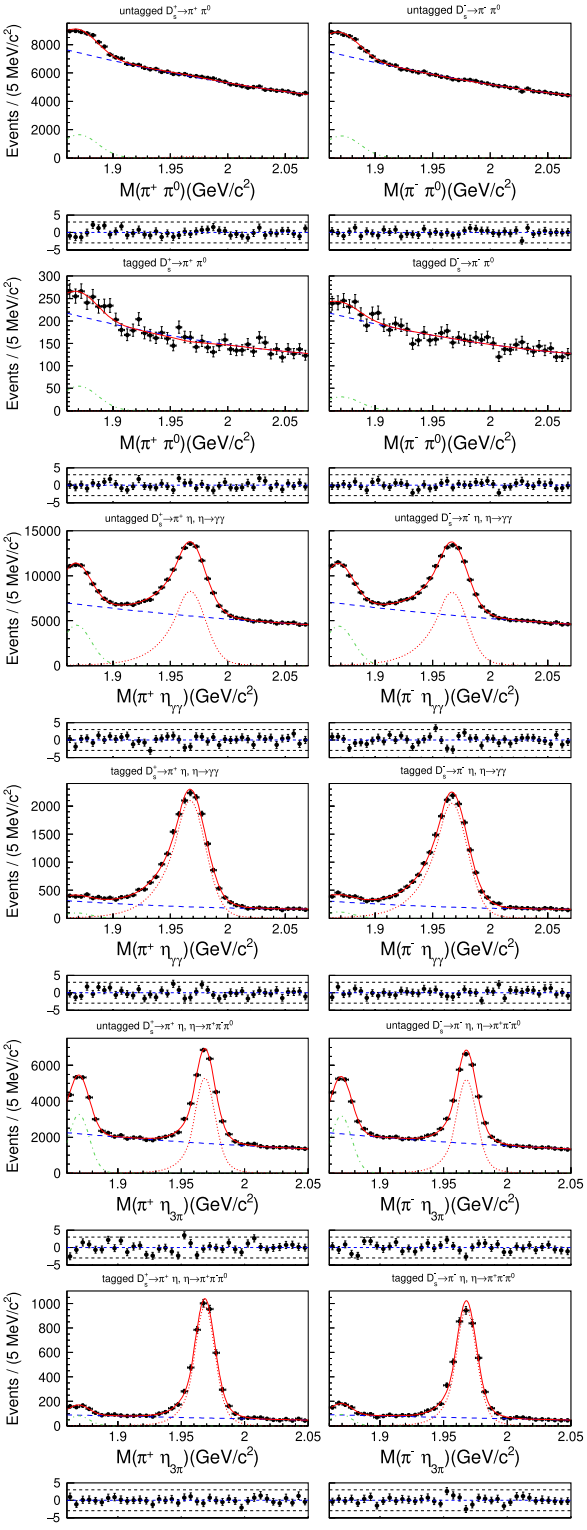

FIG. 2. Data and fit projection for $D_s^+\to\pi^+\pi^0$ (upper two rows), $D_s^+\to\pi^+\eta_{\gamma\gamma}$ (middle two rows), and $D_s^+\to\pi^+\eta_{3\pi}$ (lower two rows). Left side shows D_s^+ candidates, right side shows D_s^- candidates. For each pair of rows, top is the untagged sample, bottom is the tagged sample. The solid red line is the total fit, the dotted red line is signal, the broken green line is background from D^+, and the dashed blue line is combinatorial background. The plots beneath the distributions show the residuals.

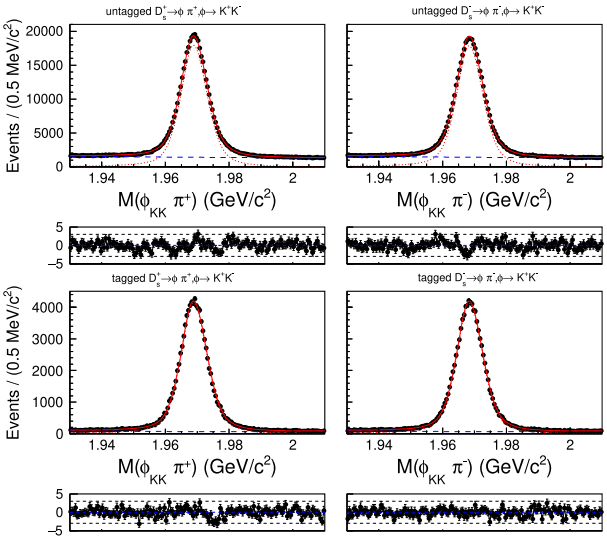

FIG. 3. Data and fit projection for the reference mode $D_s^+\to\phi\pi^+$. Left side shows D_s^+ candidates, right side shows D_s^- candidates. Upper row is the untagged sample, lower row is the tagged sample. The solid red line is the total fit, the dotted red line is signal, and the dashed blue line is background. The plots beneath the distributions show the residuals.

in both decay modes are essentially identical, the asymmetry A_ϵ is expected to be the same. As the asymmetry $A_{\rm FB}$ is independent of decay mode, subtracting the $D_s^+\to\pi^+\eta$ and $D_s^+\to\phi\pi^+$ raw asymmetries yields the difference in CP asymmetries,

$$\Delta A_{\rm raw}\equiv A_{\rm raw}^{\pi\eta}-A_{\rm raw}^{\phi\pi}=A_{CP}^{\pi\eta}-A_{CP}^{\phi\pi}. \tag{5}$$

Thus, $A_{CP}^{\pi\eta}=\Delta A_{\rm raw}+A_{CP}^{\phi\pi}$. Inserting the well-measured value $A_{CP}^{\phi\pi}=-0.0038\pm0.0026\pm0.0008$ [24] subsequently yields $A_{CP}^{\pi\eta}$.

For signal modes $D_s^+\to K^+\pi^0$ and $D_s^+\to K^+\eta$, the mode $D_s^+\to\phi\pi^+$ cannot be used to correct for A_ϵ as the K^+ and π^+ daughters are of different types. In this case, we calculate A_ϵ using previous Belle measurements of $K^\pm$ efficiencies made as a function of track momentum and polar angle [30]. We convolve this two-dimensional efficiency map with the corresponding momentum and angular distributions, as determined from MC, of the $K^\pm$ tracks in our signal modes to obtain A_ϵ. The resulting values of A_ϵ range from -0.001 to -0.008. Correcting for this asymmetry results in $A_{\rm corr}$, which is the sum of A_{CP} and $A_{\rm FB}$. As $A_{\rm FB}$ is an odd function of the polar angle $\cos\theta_{D_s}^{\rm CM}$, we extract A_{CP} and $A_{\rm FB}$ by calculating

$$\begin{aligned}A_{CP}(\cos\theta_{D_s}^{\rm CM})&=\frac{A_{\rm corr}(\cos\theta_{D_s}^{\rm CM})+A_{\rm corr}(-\cos\theta_{D_s}^{\rm CM})}{2}\\ A_{\rm FB}(\cos\theta_{D_s}^{\rm CM})&=\frac{A_{\rm corr}(\cos\theta_{D_s}^{\rm CM})-A_{\rm corr}(-\cos\theta_{D_s}^{\rm CM})}{2}.\end{aligned} \tag{6}$$

TABLE I. Reconstruction efficiencies, fitted signal yields, and resulting relative and absolute branching fractions. The yields listed are the sums of those from the tagged and untagged samples. The first and second uncertainties listed are statistical and systematic, respectively. The third uncertainty is due to the external branching fraction $\mathcal{B}_{\phi\pi^+}$. Results from the two η decay modes are combined via a weighted average and also listed. All results are corrected for the $\pi^0 \to \gamma\gamma$, $\eta \to \gamma\gamma$, or $\eta \to \pi^+\pi^-\pi^0$ branching fractions.

Decay mode	ε (%)	Fitted yield	$\mathcal{B}/\mathcal{B}_{\phi\pi^+}$ (%)	$\mathcal{B}$ (10^{-3})
$D_s^+ \to K^+\pi^0$	8.10 ± 0.04	11978 ± 846	$3.28 \pm 0.23 \pm 0.13$	$0.735 \pm 0.052 \pm 0.030 \pm 0.026$
$D_s^+ \to K^+\eta_{\gamma\gamma}$	7.42 ± 0.05	10716 ± 429	$8.04 \pm 0.32 \pm 0.35$	$1.80 \pm 0.07 \pm 0.08 \pm 0.06$
$D_s^+ \to K^+\eta_{3\pi}$	4.04 ± 0.02	3175 ± 121	$7.62 \pm 0.29 \pm 0.33$	$1.71 \pm 0.07 \pm 0.08 \pm 0.06$
$D_s^+ \to K^+\eta$	...	...	$7.81 \pm 0.22 \pm 0.24$	$1.75 \pm 0.05 \pm 0.05 \pm 0.06$
$D_s^+ \to \pi^+\pi^0$	6.63 ± 0.04	491 ± 734	$0.16 \pm 0.25 \pm 0.09$	$0.037 \pm 0.055 \pm 0.021 \pm 0.001$
$D_s^+ \to \pi^+\eta_{\gamma\gamma}$	10.84 ± 0.02	166696 ± 1173	$85.54 \pm 0.64 \pm 3.32$	$19.16 \pm 0.14 \pm 0.74 \pm 0.68$
$D_s^+ \to \pi^+\eta_{3\pi}$	6.50 ± 0.03	56132 ± 407	$83.55 \pm 0.64 \pm 4.37$	$18.72 \pm 0.14 \pm 0.98 \pm 0.67$
$D_s^+ \to \pi^+\eta$	...	...	$84.80 \pm 0.47 \pm 2.64$	$19.00 \pm 0.10 \pm 0.59 \pm 0.68$
$D_s^+ \to \phi\pi^+$	22.05 ± 0.13	1005688 ± 2527	1	...

We perform this calculation in three bins of $|\cos\theta_{D_s}^{\rm CM}|$: [0, 0.4], [0.4, 0.7], and [0.7, 1.0]. The results for A_{CP} and $A_{\rm FB}$ are plotted in Fig. 4. We subsequently fit these points to a constant to obtain final values of A_{CP}; the results are listed in Table II. For $D_s^+ \to \pi^+\pi^0$, no signal is observed, and thus there is no result for A_{CP}.

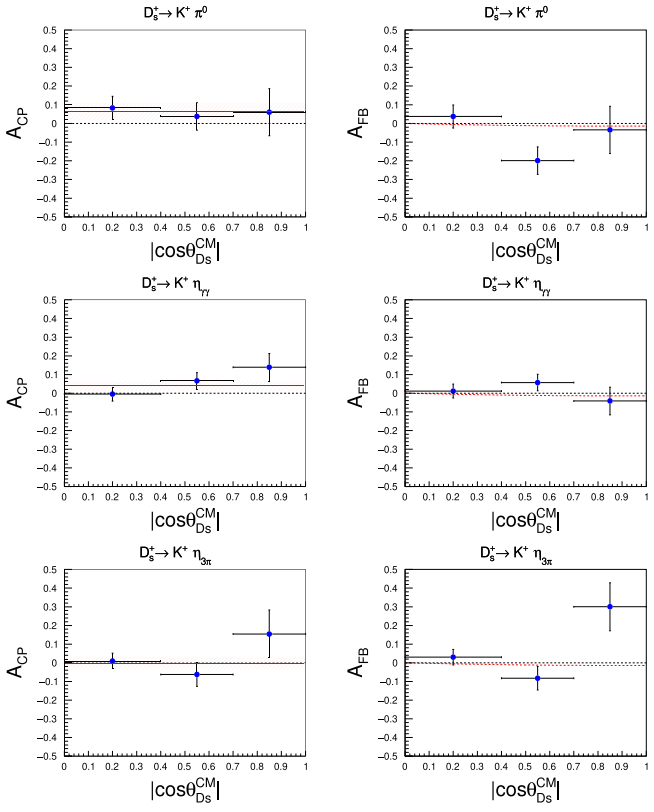

FIG. 4. *CP* asymmetries (left) and $A_{\rm FB}$ (right) in bins of $|\cos\theta_{D_s}^{\rm CM}|$, for $D_s^+ \to K^+\pi^0$ (upper), $D_s^+ \to K^+\eta_{\gamma\gamma}$ (middle), and $D_s^+ \to K^+\eta_{3\pi}$ (lower). In the plots on the left, the horizontal line shows the result of a fit to a constant, and the red shaded region shows the $\pm 1\sigma$ errors. In the plots on the right, the dashed line show the leading-order prediction [31].

The systematic uncertainties for the branching fractions are summarized in Table III. The uncertainty due to charged track reconstruction is evaluated from a study of partially reconstructed $D^{*+} \to \pi^+ D^0(\to K_S^0\pi^+\pi^-)$ decays and found to be 0.35% per track. The uncertainty due to particle identification is evaluated from a study of $D^{*+} \to \pi^+ D^0(\to K^-\pi^+)$ decays. We note that the uncertainties due to tracking and particle identification partially cancel between the signal and reference modes. The uncertainty due to $\pi^0/\eta \to \gamma\gamma$ reconstruction is evaluated from a study of $\tau^- \to \pi^-\pi^0\nu_\tau$ decays and found to be 2.4%.

To study the systematic uncertainty due to the $O_{\rm NN}$ requirement, we remove this requirement for the high-statistics $D_s^+ \to \pi^+\eta$ mode and also for the reference mode $D_s^+ \to \phi\pi^+$. We subsequently use the ${}_s\mathcal{P}lot$ [32] technique to extract the $O_{\rm NN}$ distribution for each decay. From these distributions, we calculate the efficiencies of the $O_{\rm NN}$ requirements used for the six signal decay modes. We repeat this calculation for both data and MC samples and take the difference between the resulting efficiencies as the systematic uncertainty due to the $O_{\rm NN}$ requirement.

TABLE II. Measured *CP* asymmetries. The first and second uncertainties listed are statistical and systematic, respectively. Results from the two η decay modes are combined via a weighted average and also listed.

Decay mode	$A_{\rm raw}$	A_{CP}
$D_s^+ \to K^+\pi^0$	0.115 ± 0.045	$0.064 \pm 0.044 \pm 0.011$
$D_s^+ \to K^+\eta_{\gamma\gamma}$	0.046 ± 0.027	$0.040 \pm 0.027 \pm 0.005$
$D_s^+ \to K^+\eta_{3\pi}$	-0.011 ± 0.033	$-0.008 \pm 0.034 \pm 0.008$
$D_s^+ \to K^+\eta$	...	$0.021 \pm 0.021 \pm 0.004$
$D_s^+ \to \pi^+\eta_{\gamma\gamma}$	0.007 ± 0.004	$0.002 \pm 0.004 \pm 0.003$
$D_s^+ \to \pi^+\eta_{3\pi}$	0.008 ± 0.006	$0.002 \pm 0.006 \pm 0.003$
$D_s^+ \to \pi^+\eta$	...	$0.002 \pm 0.003 \pm 0.003$
$D_s^+ \to \phi\pi^+$	0.002 ± 0.001	...

TABLE III. Systematic uncertainties for the ratio of branching fractions, in percent. The overall uncertainty is the sum in quadrature of the listed uncertainties and corresponds to the systematic uncertainty listed in Table I. The uncertainty due to fitting for $D_s^+ \to \pi^+\pi^0$ is fractionally large because the signal yield is so small.

Source	$\frac{\mathcal{B}(K^+\pi^0)}{\mathcal{B}(\phi\pi^+)}$	$\frac{\mathcal{B}(K^+\eta_{\gamma\gamma})}{\mathcal{B}(\phi\pi^+)}$	$\frac{\mathcal{B}(K^+\eta_{3\pi})}{\mathcal{B}(\phi\pi^+)}$	$\frac{\mathcal{B}(\pi^+\pi^0)}{\mathcal{B}(\phi\pi^+)}$	$\frac{\mathcal{B}(\pi^+\eta_{\gamma\gamma})}{\mathcal{B}(\phi\pi^+)}$	$\frac{\mathcal{B}(\pi^+\eta_{3\pi})}{\mathcal{B}(\phi\pi^+)}$
Tracking	0.7	0.7	⋯	0.7	0.7	⋯
Particle identification	1.8	1.8	1.9	1.9	1.9	4.0
$\pi^0/\eta \to \gamma\gamma$	2.4	2.4	2.4	2.4	2.4	2.4
$O_{\rm NN}$ requirement	1.1	1.3	1.2	1.3	1.3	1.3
D_s^{*+} fraction in ε	0.7	0.7	0.7	0.7	0.7	0.7
MC statistics	0.8	0.8	0.8	0.8	0.7	0.7
Fitting	2.2	2.6	2.4	56.2	1.5	1.2
$\mathcal{B}(\eta \to \gamma\gamma)$	⋯	0.5	⋯	⋯	0.5	⋯
$\mathcal{B}(\eta \to \pi^+\pi^-\pi^0)$	⋯	⋯	1.2	⋯	⋯	1.2
Overall uncertainty	4.1	4.4	4.4	56.3	3.9	5.2

This uncertainty ranges from 0.9% to 1.2% for the signal modes, and is 0.6% for the reference mode.

There is systematic uncertainty in the reconstruction efficiencies $\varepsilon_{\rm sig}$ and $\varepsilon_{\phi\pi^+}$ arising from a possible difference between MC and data in the fraction of D_s^+ decays originating from $D_s^{+*} \to D_s^+\gamma$. This difference is common to both signal and normalization modes and nominally cancels out in the ratio $\varepsilon_{\phi\pi^+}/\varepsilon_{\rm sig}$. However, there could be a small difference remaining if there were a difference in reconstruction efficiencies between tagged and untagged D_s^+ decays, and this difference itself deviated between signal and normalization modes. Thus, the systematic uncertainty in the ratio $\varepsilon_{\phi\pi^+}/\varepsilon_{\rm sig}$ due to such differences is found to be small, only 0.7%. The statistical errors on $\varepsilon_{\rm sig}$ and $\varepsilon_{\phi\pi^+}$ due to the limited sizes of the MC samples used to evaluate them are taken as a systematic uncertainty.

The systematic uncertainties due to the fitting procedure are evaluated as follows. *(a)* The uncertainty due to fixed parameters in the fits is estimated by varying these parameters according to their uncertainties. For each signal mode, we vary all such parameters simultaneously, repeating the fit 1000 times. We plot the fit results and take the rms of these distributions as the systematic uncertainty. *(b)* The uncertainty due to the amount of peaking background from $D^+ \to \pi^+(\pi^0/\eta)$ decays is evaluated by varying this background by $\pm 1\sigma$; the resulting changes in the signal yields are assigned as systematic uncertainties. *(c)* The uncertainty due to the choice of fitting range is evaluated by varying this range; the change in the branching fraction is assigned as a systematic uncertainty. *(d)* To evaluate potential fit bias, we perform 1000 fits to "toy" MC samples. Small differences observed between the fitted signal yields and the input values are assigned as systematic uncertainties.

The uncertainty on the branching fraction for the reference mode $D_s^+ \to \phi\pi^+$, which is taken from Ref. [24] and is external to the analysis, is taken as a systematic uncertainty. All uncertainties are added in quadrature to give, for each signal mode, an overall systematic uncertainty. These overall uncertainties are also listed in Table III.

The systematic uncertainties for A_{CP} are evaluated in a similar manner as those for the branching fraction and are summarized in Table IV. The effect of a possible CP asymmetry [24] in peaking background from $D^+ \to \pi^+(\pi^0/\eta)$ is considered as a systematic uncertainty. The uncertainty in A_{CP} due to our choice of $\cos\theta_{D_s}^{\rm CM}$ bins is evaluated by shifting the bin boundaries; the change in A_{CP} is taken as the systematic uncertainty. The uncertainty on A_{CP} for the reference mode (from Ref. [24]) is taken as a systematic uncertainty.

In summary, we have used the full Belle data set of 921 fb^{-1} to measure the branching fractions for four decay modes of the D_s^+, and CP asymmetries for three decay

TABLE IV. Systematic uncertainties for A_{CP}. The overall uncertainty is the sum in quadrature of the listed uncertainties.

Source	$K^+\pi^0$	$K^+\eta_{\gamma\gamma}$	$K^+\eta_{3\pi}$	$\pi^+\eta_{\gamma\gamma}$	$\pi^+\eta_{3\pi}$	$\phi\pi^+$
Fitting	0.0056	0.0035	0.0020	0.0005	0.0005	0.0002
$D^+ \to \pi^+(\pi^0/\eta)$ background	0.0062	0.0022	0.0031	⋯	⋯	⋯
$\cos\theta_{D_s}^{\rm CM}$ binning	0.0068	0.0028	0.0068	⋯	⋯	⋯
A_{CP} in $D_s^+ \to \phi\pi^+$	⋯	⋯	⋯	0.0027	0.0027	⋯
Overall uncertainty	0.0108	0.0050	0.0077	0.0027	0.0027	0.0002

modes. Our results for the branching fractions relative to that of the reference mode $D_s^+ \to \phi(\to K^+K^-)\pi^+$ ($\mathcal{B}_{\phi\pi^+}$) are

$$\begin{aligned}\mathcal{B}(D_s^+ \to K^+\pi^0)/\mathcal{B}_{\phi\pi^+} &= (3.28 \pm 0.23 \pm 0.13)\% \\ \mathcal{B}(D_s^+ \to K^+\eta)/\mathcal{B}_{\phi\pi^+} &= (7.81 \pm 0.22 \pm 0.24)\% \\ \mathcal{B}(D_s^+ \to \pi^+\pi^0)/\mathcal{B}_{\phi\pi^+} &= (0.16 \pm 0.25 \pm 0.09)\% \\ \mathcal{B}(D_s^+ \to \pi^+\eta)/\mathcal{B}_{\phi\pi^+} &= (84.80 \pm 0.47 \pm 2.64)\%.\end{aligned}$$

Multiplying these results by the world-average value $\mathcal{B}_{\phi\pi^+} = (2.24 \pm 0.08)\%$ [24] gives

$$\begin{aligned}\mathcal{B}(D_s^+ \to K^+\pi^0) &= (0.735 \pm 0.052 \pm 0.030 \pm 0.026) \times 10^{-3} \\ \mathcal{B}(D_s^+ \to K^+\eta) &= (1.75 \pm 0.05 \pm 0.05 \pm 0.06) \times 10^{-3} \\ \mathcal{B}(D_s^+ \to \pi^+\pi^0) &= (0.037 \pm 0.055 \pm 0.021 \pm 0.001) \times 10^{-3} \\ \mathcal{B}(D_s^+ \to \pi^+\eta) &= (19.00 \pm 0.10 \pm 0.59 \pm 0.68) \times 10^{-3},\end{aligned}$$

where the third uncertainty listed is due to $\mathcal{B}_{\phi\pi^+}$. As we do not observe any signal for $D_s^+ \to \pi^+\pi^0$, we set an upper limit on its branching fraction,

$$\mathcal{B}(D_s^+ \to \pi^+\pi^0) < 1.2 \times 10^{-4} \quad (90\%\,\text{C.L.}).$$

Our results for $D_s^+ \to K^+\eta$ and $D_s^+ \to \pi^+\pi^0$ are the most precise to date. Our result for $D_s^+ \to \pi^+\eta$ is consistent with a previous, less precise Belle result [29] and independent of it. All of these results are consistent within 2 standard deviations with world-average values [24], and also with recent results from the BESIII experiment [13]. For $D_s^+ \to (K^+, \pi^+)\pi^0$ and $D_s^+ \to \pi^+\eta$, our results agree with theory predictions [1,2,10,11]. However, for $D_s^+ \to K^+\eta$, our result is significantly higher than theory predictions.

Our results for the CP asymmetries are

$$\begin{aligned}A_{CP}(D_s^+ \to K^+\pi^0) &= 0.064 \pm 0.044 \pm 0.011 \\ A_{CP}(D_s^+ \to K^+\eta) &= 0.021 \pm 0.021 \pm 0.004 \\ A_{CP}(D_s^+ \to \pi^+\eta) &= 0.002 \pm 0.003 \pm 0.003.\end{aligned}$$

These results are the most precise to date and represent a significant improvement in precision over current world-average values [24]. They show no evidence of CP violation but are consistent with theory predictions [1,2,8], which are very small. Our improved results for branching fractions and CP asymmetries can be input into sum rules to provide more stringent predictions for CP violation in charm decays [14].

We thank the KEKB group for the excellent operation of the accelerator; the KEK cryogenics group for the efficient operation of the solenoid; and the KEK computer group, and the Pacific Northwest National Laboratory (PNNL) Environmental Molecular Sciences Laboratory (EMSL) computing group for strong computing support; and the National Institute of Informatics, and Science Information NETwork 5 (SINET5) for valuable network support. We acknowledge support from the Ministry of Education, Culture, Sports, Science, and Technology (MEXT) of Japan, the Japan Society for the Promotion of Science (JSPS), and the Tau-Lepton Physics Research Center of Nagoya University; the Australian Research Council including Grants No. DP180102629, No. DP170102389, No. DP170102204, No. DP150103061, No. FT130100303; Austrian Federal Ministry of Education, Science and Research (FWF) and FWF Austrian Science Fund No. P 31361-N36; the National Natural Science Foundation of China under Contracts No. 11435013, No. 11475187, No. 11521505, No. 11575017, No. 11675166, No. 11705209; Key Research Program of Frontier Sciences, Chinese Academy of Sciences (CAS), Grant No. QYZDJ-SSW-SLH011; the CAS Center for Excellence in Particle Physics (CCEPP); the Shanghai Pujiang Program under Grant No. 18PJ1401000; the Shanghai Science and Technology Committee (STCSM) under Grant No. 19ZR1403000; the Ministry of Education, Youth and Sports of the Czech Republic under Contract No. LTT17020; Horizon 2020 ERC Advanced Grant No. 884719 and ERC Starting Grant No. 947006 "InterLeptons" (European Union); the Carl Zeiss Foundation, the Deutsche Forschungsgemeinschaft, the Excellence Cluster Universe, and the VolkswagenStiftung; the Department of Atomic Energy (Project Identification No. RTI 4002) and the Department of Science and Technology of India; the Istituto Nazionale di Fisica Nucleare of Italy; National Research Foundation (NRF) of Korea Grants No. 2016R1D1A1B01010135, No. 2016R1D1A1B02012900, No. 2018R1A2B3003643, No. 2018R1A6A1A06024970, No. 2018R1D1 A1B07047294, No. 2019K1A3A7A09033840, No. 2019R1I1A3A01058933; Radiation Science Research Institute, Foreign Large-size Research Facility Application Supporting project, the Global Science Experimental Data Hub Center of the Korea Institute of Science and Technology Information and KREONET/ GLORIAD; the Polish Ministry of Science and Higher Education and the National Science Center; the Ministry of Science and Higher Education of the Russian Federation, Agreement No. 14.W03.31.0026, and the HSE University Basic Research Program, Moscow; University of Tabuk Research Grants No. S-1440-0321, No. S-0256-1438, and No. S-0280-1439 (Saudi Arabia); the Slovenian Research Agency Grants No. J1-9124 and No. P1-0135; Ikerbasque, Basque Foundation for Science, Spain; the Swiss National Science Foundation; the Ministry of Education and the Ministry of Science and Technology of Taiwan; and the United States Department of Energy and the National Science Foundation.

[1] H.-Y. Cheng and C.-W. Chiang, Phys. Rev. D **100**, 093002 (2019).
[2] H.-N. Li, C.-D. Lu, and F.-S. Yu, Phys. Rev. D **86**, 036012 (2012).
[3] Y. Grossman, A. L. Kagan, and Y. Nir, Phys. Rev. D **75**, 036008 (2007).
[4] Y. Grossman, A. L. Kagan, and J. Zupan, Phys. Rev. D **85**, 114036 (2012).
[5] A. Lenz and G. Wilkinson, Annu. Rev. Nucl. Part. Sci. **71**, 60 (2021).
[6] R. Aaij *et al.* (LHCb Collaboration), Phys. Rev. Lett. **122**, 211803 (2019).
[7] A. Dery and Y. Nir, J. High Energy Phys. 12 (2019) 104.
[8] F. Buccella, A. Paul, and P. Santorelli, Phys. Rev. D **99**, 113001 (2019).
[9] Charge-conjugate modes are implicitly included throughout this paper unless stated otherwise.
[10] H.-Y. Cheng and C.-W. Chiang, Phys. Rev. D **81**, 074021 (2010).
[11] F.-S. Yu, X.-X. Wang, and C.-D. Lu, Phys. Rev. D **84**, 074019 (2011).
[12] H. Mendez *et al.* (CLEO Collaboration), Phys. Rev. D **81**, 052013 (2010).
[13] M. Ablikim *et al.* (BESIII Collaboration), J. High Energy Phys. 08 (2020) 146.
[14] S. Müller, U. Nierste, and S. Schacht, Phys. Rev. Lett. **115**, 251802 (2015).
[15] I. I. Bigi and A. I. Sanda, *CP Violation* (Cambridge University Press, Cambridge, UK, 2009).
[16] A. Abashian *et al.* (Belle Collaboration), Nucl. Instrum. Methods Phys. Res., Sect. A **479**, 117 (2002); also see Section II in J. Brodzicka *et al.*, Prog. Theor. Exp. Phys. (**2012**), 04D001.
[17] S. Kurokawa and E. Kikutani, Nucl. Instrum. Methods Phys. Res., Sect. A **499**, 1 (2003), and other papers included in this Volume; T. Abe *et al.*, Prog. Theor. Exp. Phys. (**2013**), 03A001 and references therein.
[18] D. Lange, Nucl. Instrum. Methods Phys. Res., Sect. A **462**, 152 (2001).
[19] T. Sjöstrand, P. Edén, C. Friberg, L. Lönnblad, G. Miu, S. Mrenna, and E. Norrbin, Comput. Phys. Commun. **135**, 238 (2001).
[20] R. Brun *et al.*, CERN Report No. CERN-DD-EE-84-1, 1987.
[21] E. Barberio and Z. Wąs, Comput. Phys. Commun. **79**, 291 (1994).
[22] V. Babu *et al.* (Belle Collaboration), Phys. Rev. D **97**, 011101 (2018).
[23] E. Nakano, Nucl. Instrum. Methods Phys. Res., Sect. A **494**, 402 (2002).
[24] P. A. Zyla *et al.* (Particle Data Group), Prog. Theor. Exp. Phys. (**2020**), **083C01**.
[25] M. Feindt and U. Kerzel, Nucl. Instrum. Methods Phys. Res., Sect. A **559**, 190 (2006).
[26] G. Punzi, eConf **C030908**, MODT002 (2003) [arXiv: physics/0308063].
[27] T. Skwarnicki, Ph.D. Thesis, Institute for Nuclear Physics, Krakow 1986; , DESY Report No. F31-86-02, 1986.
[28] F. James, *Statistical Methods in Experimental Physics* (2nd Edition) (World Scientific Publishing Co., Singapore, 2006), pp. 73–75.
[29] A. Zupanc *et al.* (Belle Collaboration), J. High Energy Phys. 09 (2013) 139.
[30] M. Starič *et al.* (Belle Collaboration), Phys. Rev. Lett. **108**, 071801 (2012).
[31] The leading-order prediction for $A_{\rm FB}$ at $\sqrt{s} = 10.6$ GeV is $-0.029\cos\theta^{\rm CM}_{D_s}/(1+\cos^2\theta^{\rm CM}_{D_s})$. See O. Nachtmann, *Elementary Particle Physics*, (Springer-Verlag, Heidelberg, Germany, 1990).
[32] M. Pivk and F. R. Le Diberder, Nucl. Instrum. Methods Phys. Res., Sect. A **555**, 356 (2005).